Large Volume Magnetically Shielded Room and ARIADNE Candidate Component Magnetic Field Characterization

J.I. Sofair
Lafayette College, Department of Physics, Easton, PA 18045

N.Q. Aggarwal, A. Babu, A. Zamora, and HG. Berns
University of California–Davis, Department of Physics and Astronomy, Davis, CA 95616

M. Ellaqany
Furman University, Department of Physics, Greenville, SC 29613

The Axion Resonant InterAction Detection Experiment (ARIADNE) will search for the quantum chromodynamics (QCD) axion by measuring magnetic fields that manifest from these axion-mediated forces using a nuclear magnetic-resonance-based technique. The fields ARIADNE aims to measure are on the order of 10^{-20} T. To measure such minuscule magnetic fields, every piece of the ARIADNE apparatus needs to be minimally magnetic. Pursuant to this goal, we characterized the background DC and AC magnetic fields in the UC–Davis Department of Physics and Astronomy large volume magnetically shielded room (MSR), and used this information to study components that may be used in the final ARIADNE apparatus. Our measurements of the background field in the MSR revealed that the shielding material in the room is underperforming. We present these measurements of the background fields along with those of our candidate components and explore the most likely cause for the underperformance of the shielding material.

I. INTRODUCTION

The quantum chromodynamics (QCD) axion is a theoretical particle proposed to resolve the Strong Charge Parity (CP) Problem. The Strong CP Problem describes a discrepancy between theory and experiment in which charge (C) and parity (P) symmetry are expected to be broken, but they have been observed to be preserved [1, 2]. Proving the existence of the QCD axion would solve the problem by substantiating a proposed mechanism for this discrepancy. The Axion Resonant InterAction Detection Experiment (ARIADNE) aims to detect this particle using a nuclear-magnetic-resonance-based technique.

The QCD axion is predicted to mediate short-range, spin-dependent forces between fermions. If two fermions are separated by a small distance r, the axion will couple to the mass of one particle and the spin of the other. The potential of this interaction is given in [3]:

$$V_{sp}(r) = \frac{\hbar^2 g_s^N g_p^N}{8\pi m_N}\left(\frac{1}{r\lambda_a} + \frac{1}{r^2}\right) e^{-\frac{r}{\lambda_a}} (\vec{\sigma}\cdot\hat{\vec{r}}) \qquad (1)$$

where g_s^N and g_p^N are coupling constants related to the axion mass, m_N is the mass of the unpolarized nucleon, $\vec{r}$ is the vector between the polarized and unpolarized masses, $\lambda_a = \hbar/(m_a c)$ is the reduced Compton wavelength of the axion, and $\vec{\sigma}$ is the Pauli spin matrix.

The potential's dependence on $\vec{\sigma}$ means the axion coupling can be treated as an effective magnetic field. This is because $\vec{\sigma}$ is proportional to the nuclear magnetic moment of the particle. The strength of the effective magnetic field created in these QCD-axion-mediated interactions depends on the coupling constants g_s^N and g_p^N.

The r-dependence in Equation 1 further shows that changing the distance between the polarized and unpolarized masses also changes the strength of the effective magnetic field created by the axion coupling. Modulating the distance at the Larmor frequency will therefore result in precession of the polarized mass' spin [1]. If the polarized mass' spin is aligned with the z-axis, then distance modulation will cause a time-varying, non-zero component of the spin to align with the x-axis. This non-zero x-component of the spin will result in a magnetic field of magnitude $\sim 10^{-20}$ T.

ARIADNE will use ^{3}He subjected to a magnetic field $\vec{B}_{ext}$ as the polarized mass, and a rotating tungsten rotor as the unpolarized source mass (see Figure 1). Modulating the distance between these masses is made relatively simple by choosing the unpolarized mass to be a rotor. The rotor has 11 "teeth," each with a depth of 200 μm (see Figure 2). Given the number of teeth, rotating the rotor at a frequency f_{rot} = 5–9 Hz, the modulation frequency, f_{mod}, will be equal to $11 f_{rot}$. To spin the rotor, we connect the rotor to a shaft and rotate the shaft via a motor. This creates an effective magnetic field $\vec{B}_{eff} \sim 10^{-20}$ T along the x-axis via the mechanisms described above that can be measured by a superconducting quantum interference device (SQUID).

To achieve the measurements of $\vec{B}_{eff}$, every piece of the apparatus must be minimally magnetic. This work describes the steps we took to measure the magnetic properties of various candidate components for the ARIANDE apparatus. The candidate components that were measured are the Shinsei USR30-S3 motor and three types of metallic gold paint that will be used to better thermally isolate the motor in the final apparatus. All measurements were made in the UC–Davis Depart-

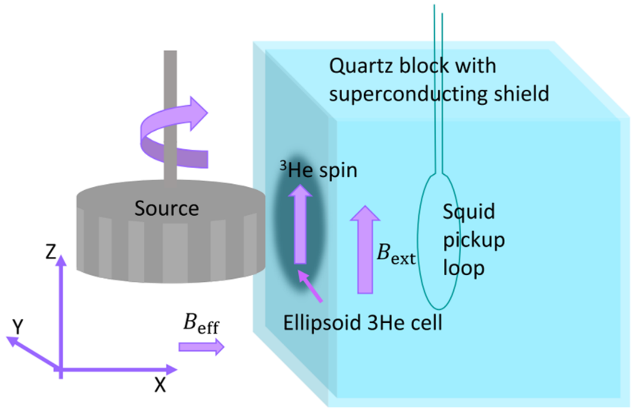

FIG. 1: High level diagram of ARIADNE (from Figure 1 of [2]). Refer to Section I for details.

FIG. 2: Tungsten rotor CAD illustration (Figure 4.27 of [1]). Notice the shallow teeth on the outermost edge. The presence of these teeth means that the distance between this rotor (the unpolarized source mass) and the ^{3}He (the polarized source mass) will change as the rotor is spun.

ment of Physics and Astronomy magnetically shielded room (MSR). Therefore, we had to characterize the background magnetic fields in the MSR before we could make any conclusive statements on the properties of the components.

In Section II, we will discuss the state of the MSR, the components that were measured, and the sensor mounts that we designed to make the measurements. Then, in Section III, we will describe how the components were measured. In Section IV, we will present and discuss our measurements, including our findings that the shielding material in the MSR underperformed.

II. SHIELDED ROOM ENVIRONMENT AND COMPONENT AND MEASUREMENT DESCRIPTION

A. Magnetically Shielded Room

The MSR has two sections: One that is unprotected from external magnetic fields (MSRa), and another that is shielded from these fields (MSRb). Within the walls and floor of MSRb are dozens of panels of high-silicon steel. These panels are what screen unwanted magnetic fields originating from the Earth and other miscellaneous external sources. The MSR was originally purposed for geophysical research, and some of the information on the room and its shielding properties was lost when the primary investigators changed.

In the Spring of 2024, the flooring in MSRb was removed to determine where the shielding material was grounded to. We learned that the shielding material is grounded in the same place as the electrical sockets in the room, the repercussion of which will be further discussed in Section IV. The consequence of the lack of flooring for this work is that the time spent inside the shielded portion of the room had to be minimized, as deforming high-silicon steel causes external magnetic fields to “leak” through. Moreover, any experimental setup in MSRb had to be sufficiently light so as to not damage the shielding panels.

Another piece of information about the MSR that had to be filled in was the shielding properties of the room. We needed to characterize the background magnetic fields in the room to properly understand the magnetic properties of the candidate components that we measured. If the background fields are too strong, we would not be able to make conclusive statements about the candidate components.

B. Components

As mentioned in Section I, the motor will be responsible for rotating the unpolarized source mass, thereby causing the distance modulation that affects the strength of the axion-mediaterd magnetic field, $\vec{B}_{eff}$. Reference [1] explored the magnetic properties of the Aerotech ADRS100 motor and found that it produces a magnetic field strong enough to interfere with ARIADNE. In this work, we measured the magnetic properties of a Shinsei USR30-S3 (see Figure 3). This motor is compact, making it compatible with the physical constraints of the ARIADNE apparatus [1]. Moreover, its advertised nonmagnetic properties make it ideal for this experiment. The results of our measurements can be found in Section IV.

The USR30-S3 can operate at a minimum temperature of roughly 263 K [4], while the coldest parts of the apparatus need to be held close to 4 K. The motor will therefore be surrounded by a G10 box to better thermally insulate

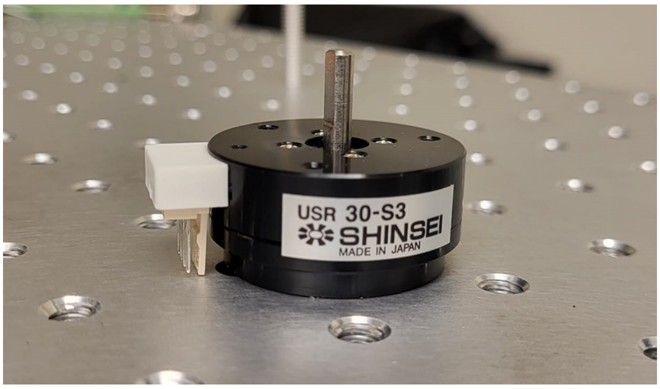

FIG. 3: The Shinsei USR30-S3 ultrasonic motor.

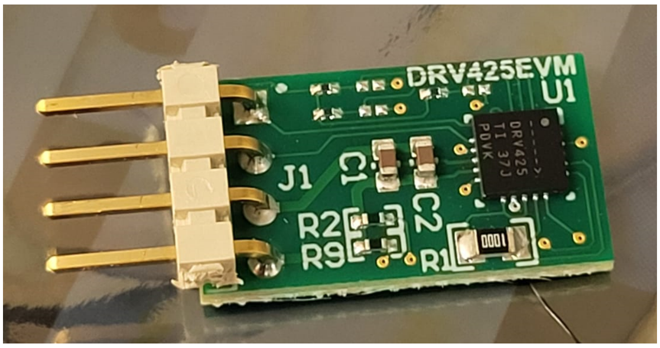

FIG. 5: The Texas Instruments DRV425EVM.

FIG. 6: The Magnetic Sciences MC90R. Image credit: Magnetic Sciences.

it. The inside faces of this box will likely be painted to improve the box's insulative properties. We tested three different metallic gold paints to see if they would be too strongly magnetic for use in ARIADNE. We chose this type of paint specifically because their emissivity should help to insulate the motor.

We applied the three different paints to three pieces of cardboard, and kept a fourth piece of cardboard unpainted to use as a control (see Figure 4). The control allowed us to ensure that the cardboard itself did not have significant amounts of ferromagnetic dirt that would have biased our conclusions about the paints. Each type of paint and their respective cardboard pieces were labelled A, B, and C.

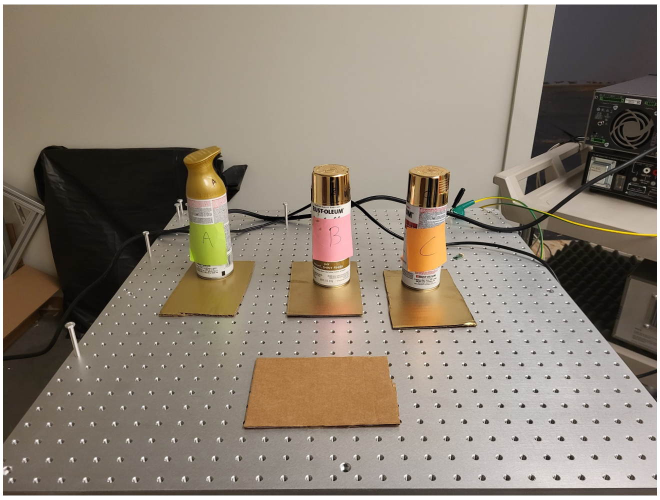

FIG. 4: The three paints chosen for this experiment atop their respective painted pieces of cardboard. The control (unpainted) piece of cardboard is pictured, as well. Each paint can is labelled from A through C with a post-it note. The cardboard pieces are labelled on their backs, as well.

C. Mount Design

To get the information we needed, we used three Texas Instruments DRV425EVM fluxgate magnetometers (see Figure 5) to measure the x-, y-, and z-axes of any DC magnetic fields and the Magnetic Sciences MC90R Hall effect sensor (see Figure 6) to measure any AC fields. The mounts for both kinds of magnetometers were designed in-house and 3D printed for testing.

The DRV425EVM mount design consists of a small PCB vise with thin enough walls to be tightened via a screw. The vise is fastened to a 6 mm diameter post with another screw, and the post is held by a post holder. Post height can be adjusted with a thumb-tightening screw. The post and post holders are modeled after the ThorLabs Mini-Series Optical Post Assembly pieces. As such, our post holder can be fastened to an optical breadboard using the ThorLabs MSC2 clamping fork. As mentioned

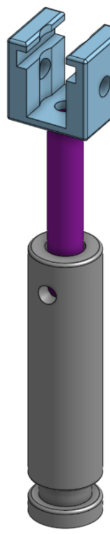

FIG. 7: DRV425EVM x- and y-axis mount design. Includes: PCB vise (light blue) to slide DRV425EVM into, post (purple) to adjust height of sensor, and post holder (gray) to fasten the entire mount to an optical breadboard.

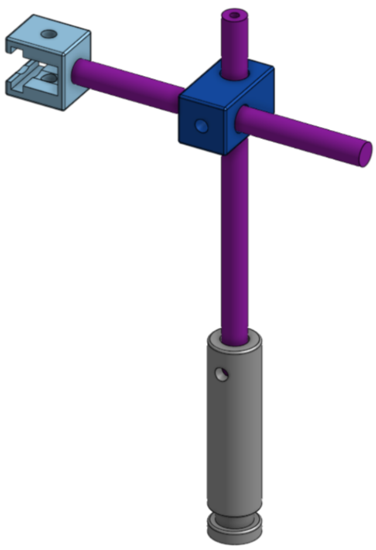

FIG. 8: DRV425EVM z-axis mount design, which includes a simple block (dark blue) that can hold two posts perpendicular to one another. The horizontal post holds the PCB vise so that the sensor can measure fields along the z-axis (i.e. perpendicular to the top of the optical breadboard).

above, we needed one magnetometer for each dimension of the magnetic field that we wanted to measure. Therefore, we needed three different mounts. See Figures 7 and 8 for CAD illustrations of the mounts.

The mount for the MC90R consists of two semi-circles that fit around the body of the sensor that can be screwed into an outer housing to achieve a finite number of measurement angles (see Figure 9). The housing can be secured to an optical breadboard by screwing in the bottom.

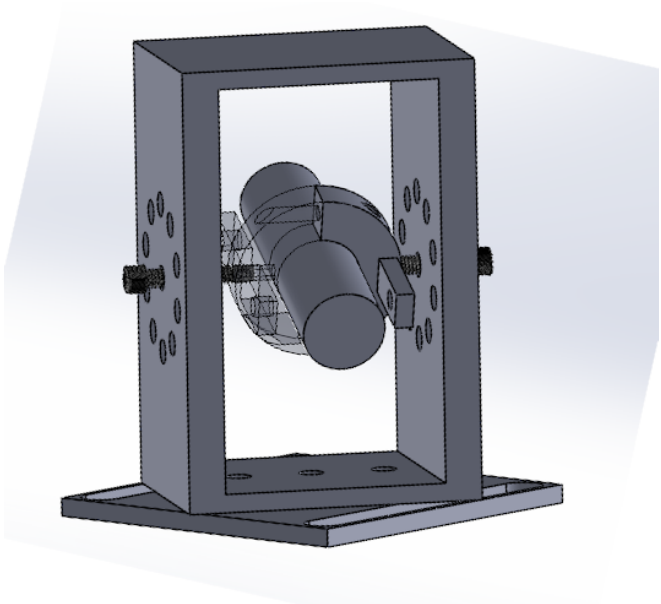

FIG. 9: MC90R sensor mount. The sensor itself is the cylinder in the middle. It is being held by the two semi-circular clamps on the side. The clamps get screwed into the outer housing, and then pins get passed into the through holes in the clamps and the outer housing to fix the sensor at one of 11 possible angles. Image and design credit: Akilan Babu.

III. MEASUREMENTS AND CALCULATIONS

In the shielded portion of the MSR, we measured the following: The background magnetic fields, the fields of the Shinsei USR30-S3, three types of metallic gold paint, and an unpainted cardboard square to serve as a control for the paint. We set up our four total magnetometers on a small optical breadboard resting atop a lightweight table in the center of the room so as to minimally disturb the exposed shielding material in MSRb. On the optical breadboard, we positioned three DRV425EVMs—one for each axis—as close to one another as possible so that they measured roughly the same point in space. We placed the MC90R nearby, as well. Figures 10 and 11 show how we configured the four magnetometers next to the motor. We used this configuration to make all of our measurements.

To measure the four pieces of cardboard, we simply slotted one piece at a time between the DRV425EVM mounts and the MC90R mount. All data were recorded for at least 10 seconds to ensure there was enough information to make strong conclusions about the characteristics of the fields we measured.

To determine the magnitude of the DC fields we mea-

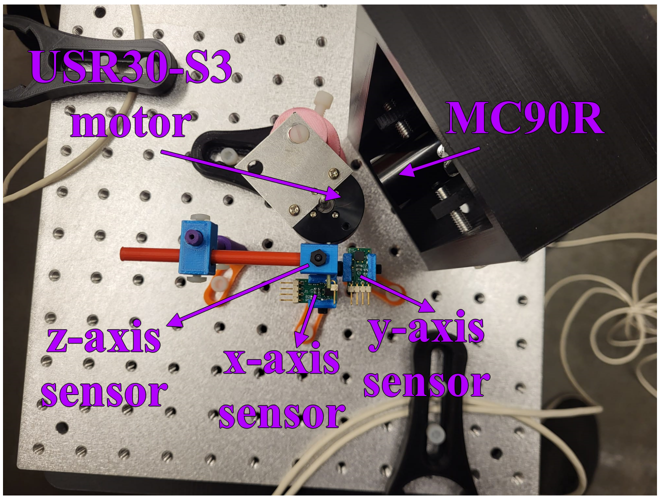

FIG. 10: Top-down view of measurement setup with relevant components labeled. The USR30-S3 motor is placed between the magnetometers for reference. None of the magnetometers are plugged in for the sake of clarity.

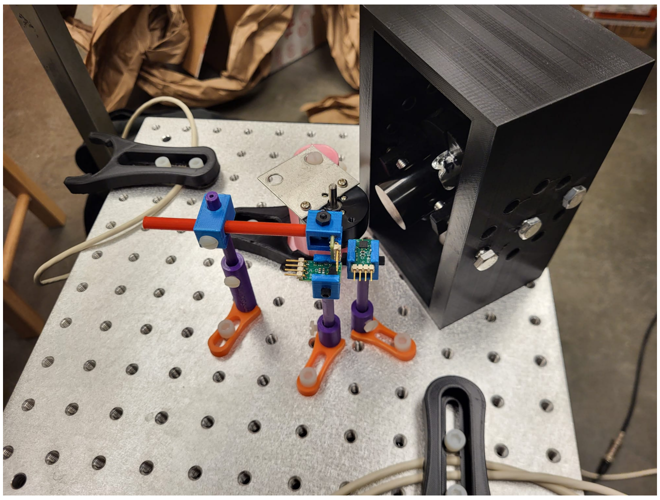

FIG. 11: Unlabelled, alternative angle of the measurement setup.

sured, we added the DRV425EVM voltage measurements at each time step in quadrature, then converted this voltage to Teslas using the following equation from the manual [5]:

$$\begin{aligned} B &= \frac{V_{out}}{G \cdot Gfg \cdot R_{shunt}} \\ &= \frac{V_{out}}{4V/V \cdot 12.2mA/mT \cdot 1000\Omega} \end{aligned} \tag{2}$$

V_{out} is the output voltage with reference to ground, so subtracting the reference voltage from V_{out} before performing any further calculations was not necessary. G and Gfg are the compensation current and the fixed gain

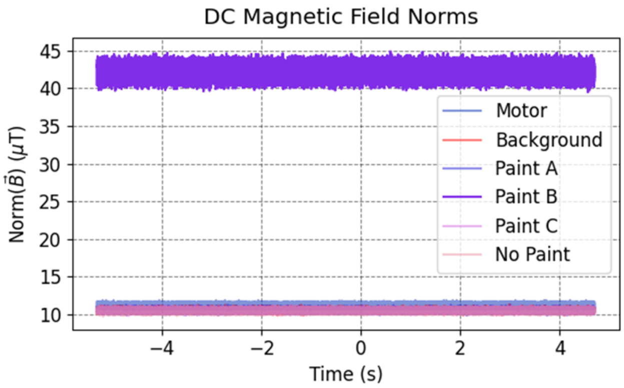

FIG. 12: DC magnetic field magnitude over time for the USR30-S3 motor, MSRb background, the three paints (A, B, and C), and the unpainted cardboard. Other than the clear outlier of paint B, all of the other measurements stayed consistently around similar values.

of a difference amplifier integrated on the DRV425EVM, respectively. R_{shunt} is the strength of an external shunt resistor. The default value for R_{shunt} is $100\,\Omega$, but this would not have given us the resolution that we needed. We therefore changed the shunt resistors on all of our DRV425EVMs to be $1000\,\Omega$.

The MC90R sensor was connected directly to a spectrum analyzer rather than an oscilloscope, so our AC field measurements come in the form of spectra. We present the results of all of our measurements and calculations in the following section.

IV. RESULTS

Figure 12 shows the norm of the DC magnetic field vector over time for each of the six measurements we performed (the USR30-S3 motor, MSRb background, the three paints (A, B, and C), and the unpainted cardboard piece that served as a control for the paints). It is clear that paint B would not be suitable for ARIADNE given the relative strength of its magnetic field compared to paints A and C. Paint B sat consistently above $40\,\mu$T, while all of the MSR and the other components were below $15\,\mu$T. This can also be seen in Figure 13, which shows a comparison of the time-averaged DC magnetic field norms for each measurement type.

These two figures reveal the unexpected fact that the background magnetic field strength is similar to that of the other fields (besides paint B). We expected the background magnetic field to be approximately 300 nT, enabling us to properly characterize the candidate components. However, the average value for the background that we observed was approximately $10.54\,\mu$T. The further tests we performed to determine the cause of this discrepancy will be discussed shortly in Section IV A.

We can also see the inefficacy of the shielding in the AC

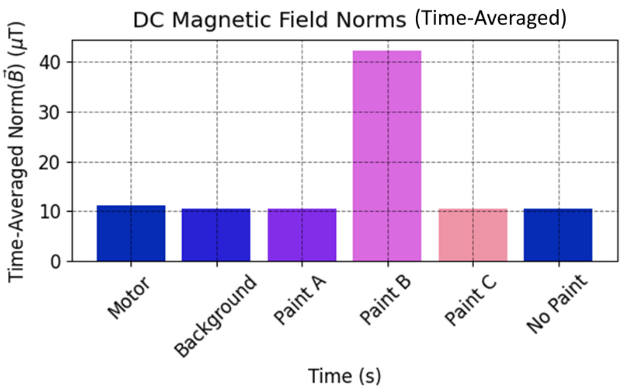

FIG. 13: Time-averaged DC magnetic field magnitude for the same six objects as in Figure 12. Once again, we see how close five of the objects were, while paint B is a definitive outlier.

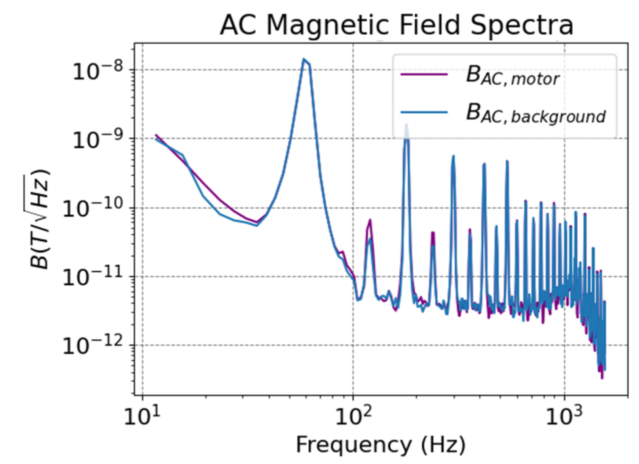

FIG. 14: AC magnetic field spectrum for the motor and the MSRb background.

field measurements. Figure 14 shows two spectra: One of the motor and one of the background. The spectra are almost identical, clearly corroborating the fact that the shielding material is underperforming.

A. Inefficacy of the High-Silicon Steel

We hypothesize that the most likely reason for the underperformance of the high-silicon steel panels in MSRb is their grounding. As mentioned in Section II, the high-silicon steel share a ground point with the electrical sockets in the room. This may have caused a small amount of current to flow through the shielding material, degrading their performance. To test if this was indeed the case, we repeated our measurements with all of the electronics in the MSR completely off and with the measurement instruments (e.g., the spectrum analyzer) outside of the room and powered with an outside socket. Unfortunately, there was not enough time to thoroughly analyze these data.

V. CONCLUSIONS AND FUTURE DIRECTIONS

This work presents measurements for the background magnetic field in the UC–Davis Department of Physics and Astronomy magnetically shielded room, as well as measurements for the magnetic field strength of candidate components for the ARIADNE apparatus. The first candidate component is a motor that will rotate the unpolarized source mass, causing the distance modulation that will make the spin of the polarized source mass precess due to the presence of the QCD axion. The other candidate components are three types of metallic gold paint, one of which will coat the inner faces of the G10 box that will help thermally insulate the motor from the rest of the apparatus.

To make all of the measurements, we used three magnetometers—one for each axis—for DC fields and a fourth magnetometer for the AC fields. We designed and printed the mounts for all of these instruments in-house. The sensors were set up on an optical breadboard on a lightweight table that we used to avoid damaging the exposed high-silicon steel shielding material in the MSR.

From our measurements, we found that paint B was significantly more magnetic than all of the other objects we measured. However, we could not make any further conclusions because of how similar the background magnetic field strength was compared to that of the components. We expected the background to be approximately 300 nT, but we measured it to be almost 30 times higher at approximately 10.54 μT. We hypothesized that the reason for this discrepancy is the fact that the shielding material in MSRb shares a ground with the electrical sockets in the room. While we took data to test this hypothesis, we did not have time to adequately analyze it in the timeframe of the program. Further research into these data is necessary to truly understand the cause for the underperformance of the shielding material.

Once the inefficacy of the high-silicon steel is solved, repeating all of the measurements we performed would prove fruitful, as the shielding would no longer be a limiting factor. Ideally further measurements would also make use of a more robust mounting scheme for the DC field sensors. The designs we created give a lot of flexibility for orienting the sensors, making it difficult to ensure each sensor is truly measuring the same point and that they are mutually orthogonal.

Aside from experimental improvements, more data should be collected on the motor. In particular, data when the motor is powered and/or rotating would allow us to more completely characterize its magnetic properties and to better compare it to the candidate motor measured in [1]. These data will also give us a better sense of how the USR30-S3 performs in a setting more similar to the intended one and to determine which motor is more suited to the ARIADNE apparatus.

[1] C. Lohmeyer, Ph.D. thesis, Northwestern University (2023).

[2] N. Aggarwal, A. Schnabel, J. Voigt, A. Brown, J. C. Long, S. Knappe-Grueneberg, W. Kilian, A. Fang, A. A. Geraci, A. Kapitulnik, et al., Physical Review Research **4**, 013090 (2022), ISSN 2643-1564, URL `https://link.aps.org/doi/10.1103/PhysRevResearch.4.013090`.

[3] J. E. Moody and F. Wilczek, Physical Review D **30**, 130 (1984), publisher: American Physical Society, URL `https://link.aps.org/doi/10.1103/PhysRevD.30.130`.

[4] Shinsei, *Ultrasonic Motor General Catalog* (2021).

[5] Texas Instruments, *DRV425 Evaluation Module User's Guide* (2015).